org/10.15392/2319-0612.2025.2945
Braz. J. Radiat. Sci., Rio de Janeiro
2025, 13(4) | 01-21 | e2945
Editor: Prof. Dr. Bernardo Maranhão Dantas
Editor: Prof. Dr. Alfredo Lopes Ferreira Filho
Submitted: 2025-05-21
Accepted: 2025-11-10

Applying Deep Learning in gamma-spectroscopy for radionuclide identification

Otero[a*], A. G. L.; Potiens Jr.[a]; A. J.; Marumo[a], J. T.

[a]Instituto de Pesquisas Energéticas e Nucleares, IPEN - CNEN/SP, Av. Professor Lineu Prestes 2242, Postal Code 05508-000, São Paulo, SP, Brazil

*Correspondence: aglotero@alumni.usp.br

Abstract: This study presents the results of using a Deep Convolutional Neural Network model on gamma spectrum classification for radioactive waste management. The approach uses a modified version of the VGG-19 architecture, originally developed for image recognition with 1000 mutually exclusive classes. The modified VGG-19 architecture uses a gamma spectrum as input and classifies, on a nonexclusive basis, ten classes representing the ten most common radionuclides at IPEN's Radioactive Waste Management Department (Am-241, Ba-133, Cd-109, Co-57, Co-60, Cs-137, Eu-152, Mn-54, Na-22, Pb-210). Gamma spectra were generated using Monte Carlo simulations created with PENELOPE/PenEasy, simulating an HPGe detector with sources inside a steel drum filled with paper, representing the common content of the drums managed at IPEN's Radioactive Waste Management Department. The data set was augmented by mixing these simulated spectra into new spectra containing up to four radionuclides. Several distances from the detector to the drum (41 cm, 46 cm, 51 cm, and 56 cm) were used to create a representative data set. The data from 56 cm (originally 150 spectra after the argumentation process, 375 spectra) was used for validation. After 250 training epochs, the model achieved consistent performance in the training set, demonstrating the efficiency of the method.

Keywords: Deep learning, Nuclide identification, Automated Isotope Identification, Gamma Spectroscopy, Transfer Learning, Monte Carlo Simulation.

BJRS
BRAZILIAN JOURNAL OF RADIATION SCIENCES

doi.org/10.15392/2319-0612.2025.2945
Braz. J. Radiat. Sci., Rio de Janeiro
2025, 13(4) | 01-21 | e2945
Editor: Prof. Dr. Bernardo Maranhão Dantas
Editor: Prof. Dr. Alfredo Lopes Ferreira Filho
Submitted: 2025-05-21
Accepted: 2025-11-10

Aplicação de Redes Neurais Profundas em espectroscopia gama para identificação de radionuclídeos

Resumo: Este estudo apresenta os resultados do uso de um modelo de Rede Neural Convolucional Profunda na classificação do espectro gama para gerenciamento de resíduos radioativos. A abordagem usa uma versão modificada da arquitetura VGG-19, desenvolvida originalmente para reconhecimento de imagens com 1000 classes mutuamente exclusivas. A arquitetura VGG-19 modificada usa um espectro gama como entrada e classifica, de forma não exclusiva, dez classes que representam os dez radionuclídeos mais comuns no Departamento de Gerenciamento de Resíduos Radioativos do IPEN (Am-241, Ba-133, Cd-109, Co-57, Co-60, Cs-137, Eu-152, Mn-54, Na-22, Pb-210). Os espectros gama foram gerados por meio de simulações de Monte Carlo criadas com o PENELOPE/PenEasy, simulando um detector HPGe com fontes dentro de um tambor de aço preenchido com papel, representando o conteúdo comum dos tambores gerenciados pelo Departamento de Gerenciamento de Resíduos Radioativos do IPEN. O conjunto de dados foi aumentado pela mistura dessas simulações em novos espectros contendo até quatro radionuclídeos. Várias distâncias do detector ao tambor (41 cm, 46 cm, 51 cm e 56 cm) foram usadas para criar um conjunto de dados representativo. Os dados de 56 cm (originalmente 150 espectros após o processo de argumentação, 375 espectros) foram usados para validação. Após 250 épocas de treinamento, o modelo obteve desempenho consistente no conjunto de treinamento, demonstrando a eficiência do método.

Palavras-chave: Redes Neurais Profundas, Identificação de Radionuclídeos, Identificação Automatizada de Isótopos, Espectrometria Gama, Transferência de Aprendizado, Simulações de Monte Carlo.

SBPR

1. INTRODUCTION

Neural networks, particularly deep neural networks [1], are used nowadays with great success in several tasks, such as image classification [2], image segmentation [3], translation [4], text-to-speech [5], and speech-to-text [6], achieving superhuman performance.

This study explores the capabilities of deep neural networks in the field of gamma spectroscopy analysis.

As mentioned by SUN, C. et al, 2017 [7], the success of deep learning techniques in the computer vision domain can be attributed to (a) models with high capacity, (b) increased computational power, and (c) availability of large-scale labeled data.

Transfer Learning is the application of one model in a new task, different from the one initially assigned [8]. Using a well-known deep neural network architecture called VGG-19 [2], minor modifications were made to adapt to our problem; this new network is called VGG-19-γ.

Applying Transfer Learning is a way to assess whether these models for computer vision can be extrapolated to gamma spectroscopy analysis.

Previous work investigates the properties of neural networks in gamma spectroscopy characterization, using different input methods: reducing the input size by averaging ten by the channel [9], identifying the peaks in the spectra to use as input [10] and the K-L transformation (a kind of signal compression technique) on the input spectrum [11]. The newest work [12] uses a neural network with all 1014 channel data.

These attempts pre-process the gamma spectra to reduce the input size. Applying a deep learning architecture allows us to use the original raw data directly from the detector, although deep learning models take advantage of large datasets.

Metropolis, N., and Ulam, S. [13] formalized the Monte Carlo method, introducing the concept of using random sampling to solve deterministic problems, a technique that has since become a cornerstone of computational science. In this work, the PENELOPE/penEasy[14] Monte Carlo simulation software suite was used to create a large dataset for training and testing the model in a short period of time, compared to the necessary time needed for data acquisition with a detector and a real drum.

The goal of this study was to create and validate a Deep Learning model for radionuclide identification in gamma spectroscopy. The data used for training and testing were generated using PENELOPE/penEasy [14] Monte Carlo simulations, and the validation was made using real spectra acquired at IPEN's Radioactive Waste Management Department.

2. MATERIALS AND METHODS

Artificial neural networks are software models that mimic the behavior of a biological brain on a small scale. The biological brain comprises billions of neurons and their connections, called synapses.

In software, we group artificial neurons into layers; each neuron is usually fully connected with all other neurons in the layer. Artificial neural networks generally have three layers: input, hidden, and output layers.

To simulate the synapses, a function called the activation function is applied. In artificial neural networks, the Sigmoid activation function is commonly used.

Equation 1: Sigmoid Activation Function

$$S(x) = \frac{1}{1 + e^{-x}}$$

Source: the authors.

This function takes the inputs of the neurons, aggregates the inputs, and outputs a single value. This output indicates whether the neuron is triggered (on) or not (off). Different activation functions are used depending on the data, the expected behavior, and the experimentation results.

The data flows from the input layer through several layers until the output layer represents the model output. The model output can be a continuous variable in the case of a regression or a discrete variable in the case of a classifier. In this work, a classifier was built. This classifier receives one gamma spectra input and outputs the probability that each of the ten radionuclides appears in the input spectra.

The VGG-19 [2] network architecture, shown in Figure 1, won the ImageNet Challenge 2014; it uses 47 layers to classify photos into 1000 different classes.

Figure 1: Original VGG-19 network architecture

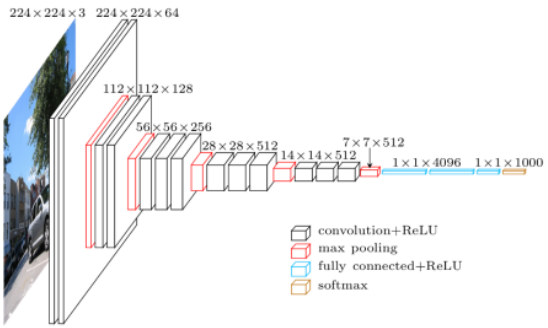

Source: Simonyan, K and Zisserman, A [2]

This architecture applies the ReLU [15] activation function as the activation function in inner connected layers, and the final layer (output) uses the Softmax activation function [16].

Equation 2: ReLU activation function

$$ReLU(x) = max(0, x)$$

Source: Householder and Alston S. [15]

Equation 3: Softmax activation function

$$\sigma(z_i) = \frac{e^{z_i}}{\sum_{j=1}^{k} e^{z_j}}, k = 1,2,\ldots,K$$

Source: Bridle, John S. [16]

The PENELOPE/penEasy [14] Monte Carlo software suite was used to simulate spectra in slightly different geometries. The base geometry consists of a) a steel drum filled with paper and the nuclear waste content (the usual content at real drums managed by the laboratory), b) a source positioned inside and at the middle of the drum, and c) an HPGe detector.

The simulation and geometry parameters have ten different radionuclides, four different detector-to-drum distances (41 cm, 46 cm, 51 cm, and 56 cm) matching the standard procedure for data acquisition at the IPEN's Waste Management Unit, five multichannel energy starts (0.01 eV, 5 eV, 10 eV, 30 eV, and 40 eV) due to equipment calibration loss due to harsh environment where the equipment set reside, and three different numbers of stories to be simulated (1.0e07, 1.0e08, and 1.0e09) as different seeds are used for each simulation, the dataset has a diverse level of confidence, this noise helps the model to learn on datapoints with different quality of measurement, resulting in 600 simulated spectra. These simulation parameters mimic the physical setup of the IPEN's Radioactive Waste Management Department.

The PENELOPE/PenEasy [14] software suite was compiled locally using the Intel® Fortran Compiler 19.0 for Linux on Ubuntu 16.04. The processor model is an Intel(R) Core(TM) i7-8700K CPU @ 3.70GHz, with 12 threads. Fifteen days of wall clock time were spent on all 600 simulations, or approximately one hundred and nine days of CPU time.

The PENELOPE/PenEasy [14] software suite allows only one source per simulation configuration, to enable training and testing with several radionuclides in one spectrum; the data set was augmented by combining different spectra into a new one.

The software environment is a Python 3.7.4 environment, Keras 2.3.0 [18], and Tensorflow-GPU 2.0.0 [19]. For deep learning hardware support, the Nvidia CUDA [20] and cuDNN [21] libraries were used. To train and test the model, the GPU code runs on a Nvidia GTX 1080 with 8 GB of VRAM.

2.1. Data generation

A data set was created using the ten most common radionuclides in the Radioactive Waste Management Department of IPEN.

A gamma spectrum is a histogram in which the number of events per energy interval is counted, each energy interval is a bin, and all bins have the same size. These spectra are the output of the simulations/measurements.

The PENELOPE/penEasy [14] software suite uses two files to run a simulation: 1) An Input File with several parameters for the Monte Carlo simulation, and 2) a geometry file containing the geometry definition used during the simulation. Table 2 summarizes the parameters used by the tallyPulseHeightSpectrum tally to generate the data, and Table 3 summarizes the detector physical characteristics that were in the geometry configuration file.

Table 1 : Ten most common radionuclides at IPEN's Radioactive Waste Management Department

Radionuclide	Energy peaks (keV) and intensity*	Source
Am-241	59.5412 (35.9%)	Dismantling lightning arresters and smoke detectors
Ba-133	80.9971 (34.06%) 276.398 (7.164%) 302.853 (18.33%) 356.017 (62.05%) 383.851 (8.94%)	Gamma source in multiphase flow meters used in the oil and gas industry
Cd-109	88.04 (3.61%)	Industrial use
Co-57	14.41300 (9.16%) 122.0614 (85.60%) 136.4743 (10.68%)	Standards and sources for calibration of radiometric equipment and medical gamma-cameras

Radionuclide	Energy peaks (keV) and intensity*	Source
Co-60	1173.237 (99.97%) 1332.501 (99.98%)	Industrial (calibration sources, gauges) and medical uses
Cs-137	661.657 (85.1%)	Industrial (calibration sources, gauges) and medical uses
Eu-152	121.78 (28.58%) 244.70 (7.580%) 344.28 (26.5%) 778.90 (12.94%) 867.37 (4.245%) 964.08 (14.60%) 1085.9 (10.21%) 1112.1 (13.64%) 1408.0 (21.00%)	Industrial (calibration sources) and medical uses
Mn-54	834.848 (99.976%)	Industrial
Na-22	1274.53 (99.944%)	Medical uses
Pb-210	46.539 (4.25%)	Industrial

Source: the authors and Karlsruhe Nuclide Chart [15]

Table 2 : penEasy simulation parameters

Parameter name	Value
STATUS	**ON**
DETECTION MATERIAL	**4 (this is the Ge inside the detector cylinder)**
EMIN	**0**
EMAX(eV)	**2059161**
No. OF E BINS	**16383**

Source: the authors

Table 3 : The Canberra GC4020 detector physical characteristics

Characteristic	Value
Diameter	**62.1 mm**
Length	**58 mm**
Distance from window	**4.5**
Window thickness	**1.50 mm**
Active volume	**153 cc**

Source: the authors and detector purchase datasheet

A Python script was developed to create the necessary Input and Geometry files to carry out all the simulations described in the section Methods. This resulted in 600 folders containing one Input and one Geometry file with the correct parameters (radionuclide, detector-to-drum distance, multichannel analyzer energy start, and number of stories).

The simulations adjust the Multi-channel Analyzer energy start to match the physical equipment's characteristics, which changes the energy start time over time, necessitating constant recalibration. This shift occurs because of the harsh environment to which the equipment is being exposed at Ipen's Radioactive Waste Management Department.

The PENELOPE/PenEasy [14] software uses the PenNuc [22] package to simulate the entire nuclear disintegration chain. This provides a more accurate simulated spectrum.

The base geometry, shown in Figure 2, consists of an HPGe detector and a steel drum; the position of the source is a parameter in the input file. Table 4 describes the materials, with their composition, that are used by the bodies described in the geometry file.

Figure 2 : Physical detector setup (left) and simulated detector setup (right)

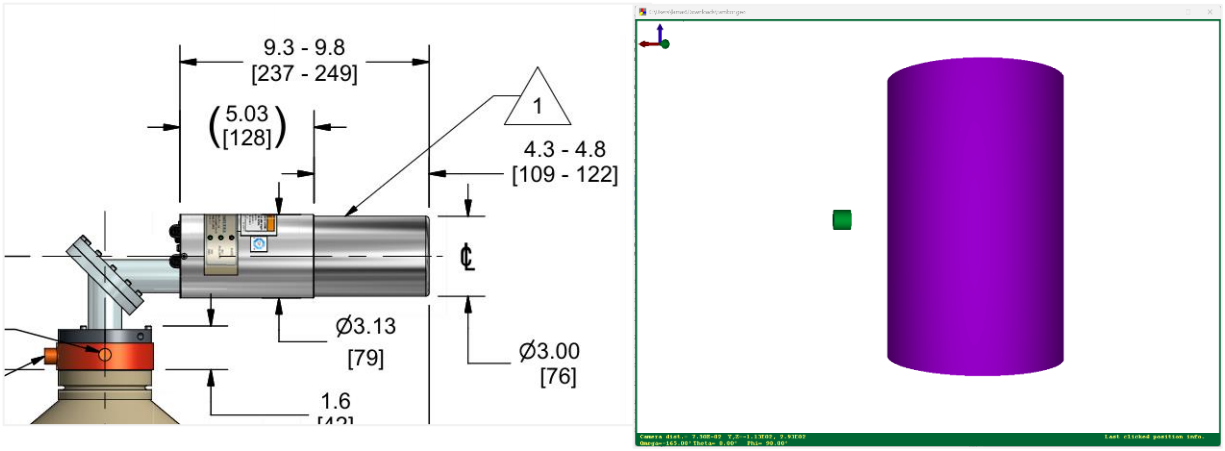

Source: Canberra GC4020 detector datasheet and the authors.

Table 4 : Geometry materials settings

Material number	Description	Material composition
1	Carbon steel (ASTM A366 1008 standard) is used on the drum	Iron (Fe) 99% Carbon (C) 0.08% Manganese (Mn) 0.6% max Phosphorus (P) 0.035% max Copper (Cu) 0.2% min Sulfur (S) 0.04%
2	Paper (the drum is usually filled with paper and the waste)	Oxygen (O) 49.34% Carbon (C) 44.44% Hydrogen (H) 6.22%
3	inner rod of the detector head, used for cooling	Copper (Cu)
4	The detector crystal itself	Germanium (Ge)
5	The detector has a beryllium window to seal the inner part of the tube with a vacuum	Beryllium (Be)
6	Surrounding air	The atmosphere that fills the space between the drum and the detector.

Source: the authors.

The simulation output is the readings for a simulated Multichannel Analyzer with 16384 channels and a maximum energy of 2.3 MeV.

2.2. Data augmentation

The data augmentation procedure consists of summarizing one randomly selected single radioisotope spectrum (from the first 600 simulated) with up to four different spectra, respecting the simulation characteristics (detector distance from the drum, number of particles simulated, and the initial energy of the Multichannel Analyzer).

Figure 3 shows an example of the final augmented data; on the left, the common histogram representation, and on the right, the same data are reshaped to a monochannel image of 128 by 128 pixels.

The reshaped process re-accommodates the vector data from the simulations (1-D) to a matrix (2-D), e.g. the vector $[0, 12, 90, 8]$ is reshaped to $\begin{bmatrix} 0 & 12 \\ 90 & 8 \end{bmatrix}$ matrix. This step is necessary because the VGG-19 architecture expects an image that is a 2-D structure.

Figure 3 : An instance of a simulation with Cs-137. As a histogram (left) and as a reshaped image (right)

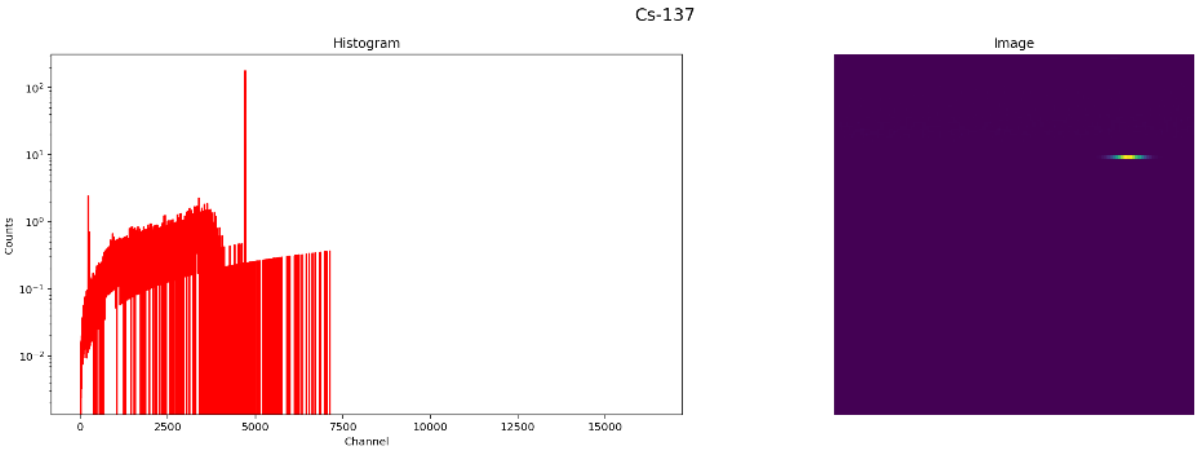

Source: the authors.

Table 5 summarizes the number of radionuclides per instance in each data set. The groups with one radionuclide came from the Monte Carlo simulations, whereas the others came from the augmentation procedure.

Table 5: Train and Test set instances per number of radionuclides on each spectrum

Number of radionuclides	Number of instances in each set	
	Train	**Test**
1	1789	597
2	3084	1016
3	4647	1521
4	3520	1232
Total instances	13040	1920

Source: the authors.

2.3. Experimental data collection

Experimental data were collected using sealed sources for the ten radionuclides and the real HPGe detector from IPEN's Radioactive Waste Management department. These ten spectra were used for validation after training and exporting the model for inference.

2.4. Modified VGG-19 architecture.

The original architecture expects an image with three channels (Red, Green, and Blue) with 224 by 224 pixels, outputting the predictions using the Softmax activation function.

The Softmax activation function is often used in the final layer of a neural network-based classifier. It takes as input a vector z of K real numbers and normalizes it into a probability distribution consisting of K probabilities proportional to the exponentials of the input numbers. After applying the function, each component will be in the interval [0, 1], and the components will add up to one, so they can be interpreted as probabilities. All components are mutually exclusive; for example, there is only one true answer at the final layer of the neural network. For example, if the classifier classifies pet photos and the possible classes are dog, cat, and bird, each image can contain only one dog, cat, or bird, not a combination of pets.

Our VGG-19-γ architecture expects a one-channel image with 128 by 128 pixels, outputting the predictions using the Sigmoid activation function. Using this function in the final layer of a neural network-based classifier allows the network to produce non-mutually exclusive components. This non mutually exclusive property allows the neural network to output multiple true values. For example, if the classifier classifies pet photos and the possible classes are dog, cat, and bird, each image can contain any combination of dog, cat, and bird.

The use of the Sigmoid Activation Function allows us to identify any combination of the ten radionuclides in the gamma spectra.

2.5. Training parameters

The train used Adam [23] as the optimizer, using 0.0001 as an initial learning rate for 250 epochs with a batch size of 8 instances per batch and binary cross-entropy as loss functions.

The total training time was 80 minutes, an average of 19 seconds per epoch. After training, the model was exported to a Keras-saved model format for reuse. The default 0.5 threshold was used; the total test time to analyze all 375 test instances using the available GPU was 3.95 seconds.

3. RESULTS AND DISCUSSIONS

After 250 epochs of training, the classification error in the training and test data sets reached a minimum, and the accuracy reached a maximum. Figure 4 shows a steady improvement in accuracy and loss metrics for training and test sets, epoch after epoch.

Figure 4 : Model Accuracy and Loss during training for train and test datasets.
Source: the authors.

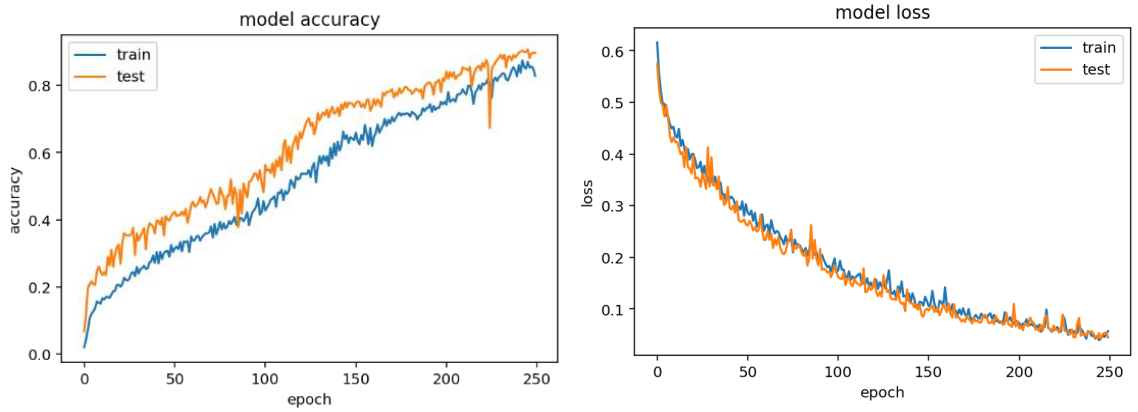

Figure 5 shows the model inference results on one test instance that was augmented, containing Ba-133 and Eu-152. In this particular case, the model classifies the correct radionuclides with a high score.

Figure **6** shows the inference results for spectra collected with the physical setup.

Figure 5: Inference result from a test instance containing Ba-133 and Eu-152. Histogram view left, image view right, and inference results bottom table

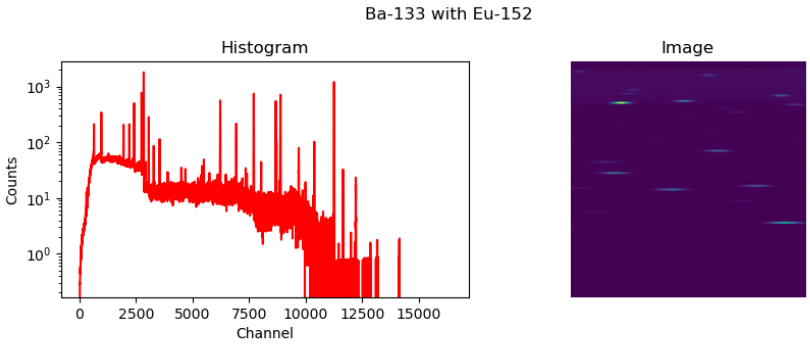

radionuclide	score	radionuclide	score
Am-241	12.57	Ba-133	99.88
Cd-109	20.65	Co-57	9.66
Co-60	2.66	Cs-137	8.21
Eu-152	99.99	Mn-54	6.53
Na-22	7.81	Pb-210	14.28

Source: the authors.

Figure 6: Inference result from spectra acquired using the physical setup. Histogram view left, image view right, and inference results bottom table

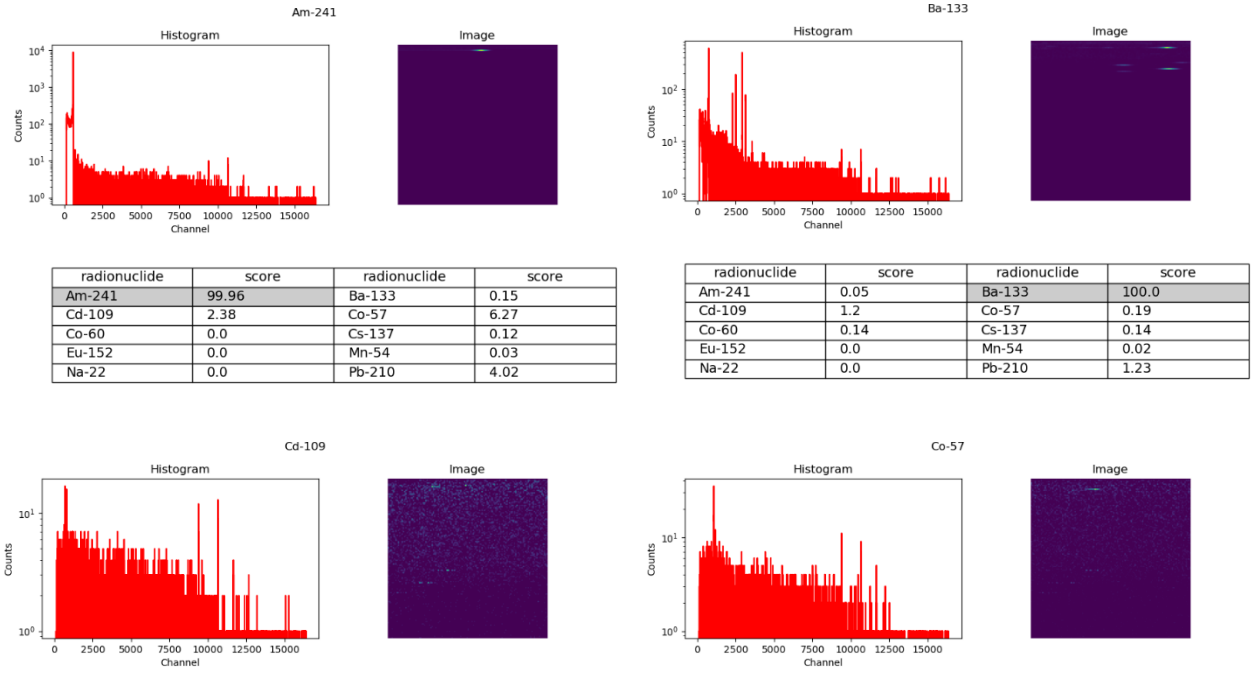

radionuclide	score	radionuclide	score
Am-241	99.96	Ba-133	0.15
Cd-109	2.38	Co-57	6.27
Co-60	0.0	Cs-137	0.12
Eu-152	0.0	Mn-54	0.03
Na-22	0.0	Pb-210	4.02

radionuclide	score	radionuclide	score
Am-241	0.05	Ba-133	100.0
Cd-109	1.2	Co-57	0.19
Co-60	0.14	Cs-137	0.14
Eu-152	0.0	Mn-54	0.02
Na-22	0.0	Pb-210	1.23

radionuclide	score	radionuclide	score
Am-241	5.26	Ba-133	1.15
Cd-109	20.61	Co-57	6.95
Co-60	0.07	Cs-137	0.56
Eu-152	0.57	Mn-54	0.37
Na-22	0.23	Pb-210	10.15

radionuclide	score	radionuclide	score
Am-241	0.32	Ba-133	0.08
Cd-109	0.62	Co-57	99.94
Co-60	0.02	Cs-137	0.03
Eu-152	0.0	Mn-54	0.56
Na-22	0.14	Pb-210	0.92

Co-60

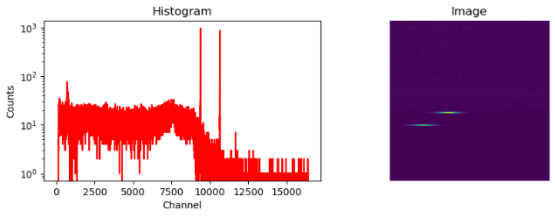

radionuclide	score	radionuclide	score
Am-241	1.42	Ba-133	0.68
Cd-109	3.21	Co-57	3.93
Co-60	99.99	Cs-137	0.61
Eu-152	0.17	Mn-54	0.73
Na-22	0.35	Pb-210	3.73

Cs-137

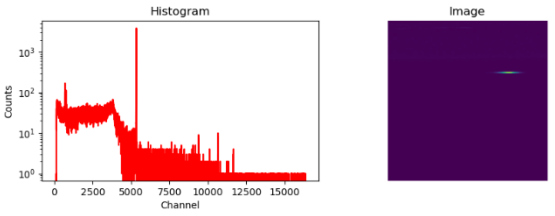

radionuclide	score	radionuclide	score
Am-241	0.63	Ba-133	1.8
Cd-109	6.25	Co-57	0.71
Co-60	0.0	Cs-137	100.0
Eu-152	0.0	Mn-54	0.01
Na-22	0.01	Pb-210	1.49

Eu-152

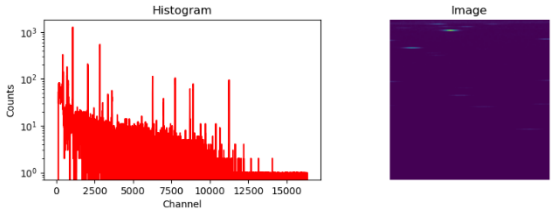

radionuclide	score	radionuclide	score
Am-241	0.02	Ba-133	0.02
Cd-109	0.08	Co-57	0.24
Co-60	0.0	Cs-137	0.04
Eu-152	100.0	Mn-54	0.04
Na-22	0.01	Pb-210	0.06

Mn-54

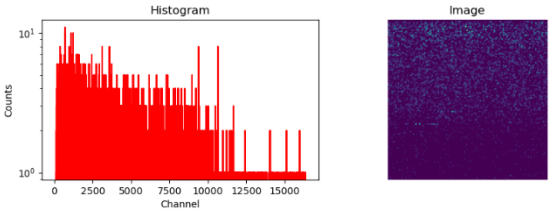

radionuclide	score	radionuclide	score
Am-241	0.15	Ba-133	0.07
Cd-109	0.13	Co-57	0.34
Co-60	0.01	Cs-137	0.05
Eu-152	0.0	Mn-54	100.0
Na-22	0.01	Pb-210	0.1

Na-22

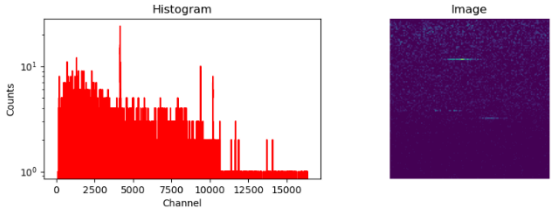

radionuclide	score	radionuclide	score
Am-241	1.75	Ba-133	0.5
Cd-109	3.31	Co-57	2.57
Co-60	0.0	Cs-137	0.08
Eu-152	0.02	Mn-54	0.06
Na-22	100.0	Pb-210	4.48

Pb-210

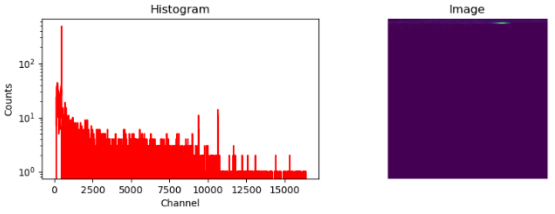

radionuclide	score	radionuclide	score
Am-241	1.46	Ba-133	0.08
Cd-109	2.1	Co-57	0.99
Co-60	0.0	Cs-137	0.09
Eu-152	0.0	Mn-54	0.04
Na-22	0.01	Pb-210	99.13

Source: the authors.

Using the test data, a receiver operating characteristic (ROC) [24] curve analysis was performed to assess the relationship between the threshold for each class and the true positive rate / false positive rate.

The Youden's J statistic method was used to select the optimal threshold. It was computed by using the numpy roc_curve output, selecting the threshold that maximizes the difference between True Positive Rate and False Positive Rate. Figure 7 summarizes the ROC

curves for each class. Several classes present True Positive Rate = 1 and False Positive Rate = 0 at the test dataset, thus those curves overlap. Cd-109 and Pb-210 are visible in the chart due to the True Positive Rate and False Positive Rate not being one.

Figure 7 : ROC curve and thresholds for each class.

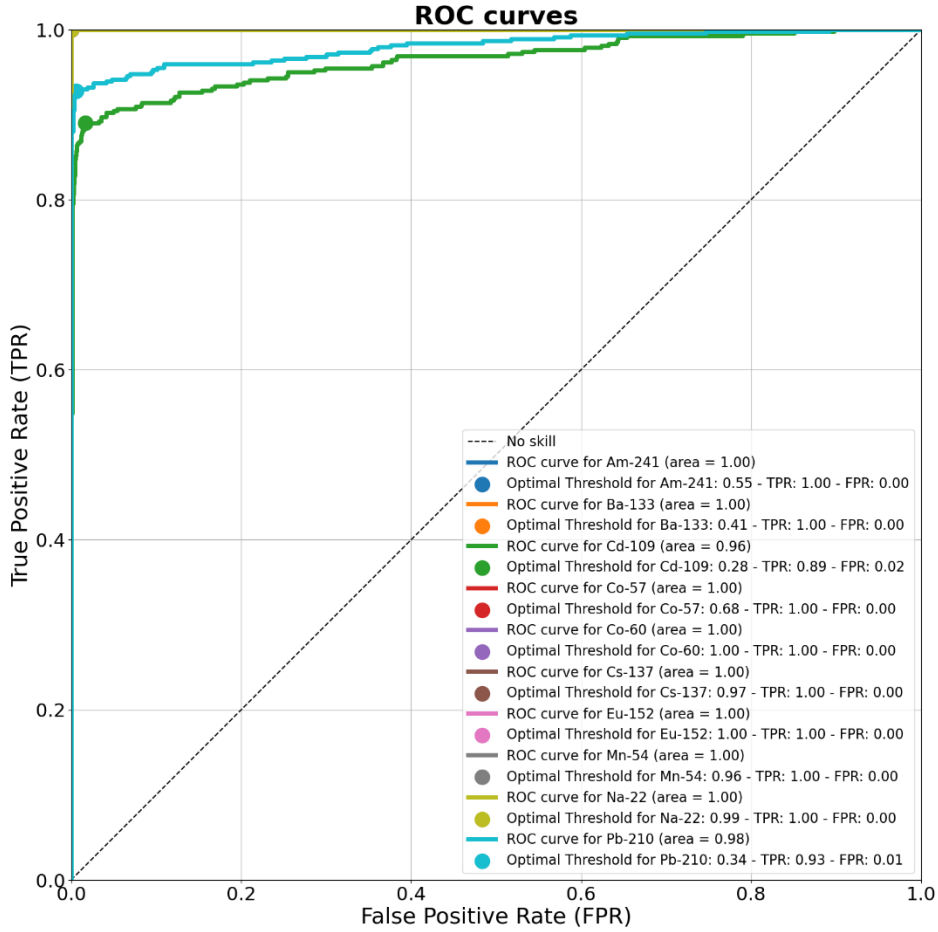

Source: the authors.

The method proposed by Keller et al. (1995) reduces from 512 spectra channels to 20, averaging ten by ten channels from the channel interval 40 to 239 [9]. The output is the probability of occurrence for eight radionuclides. Keller et al. (1995) report a great performance on spectra with one or two radionuclides, although the size of the training set is unspecified; thus, there is no way of validating the results.

The method proposed by Yoshida, E. et al. [10] reduces the 4096-channel spectra to a 47-channel input, applying a peak search procedure to feed the input of the neuron

network. The output is the probability of occurrence for 28 radionuclides. This method performs well on spectra with up to three radionuclides.

The method proposed by Liang Chen and Yi-Xiang Wei [11] reduces the 1024-channel spectra to a 64-channel input, applying a K–L transform that is a particular orthogonal transform used mainly to compact the data for 1D and 2D signals. The output is the probability of occurrence for eight radionuclides. Although the authors report precise results, only 96 measurements were performed, and the same data were used for training and testing, invalidating the test procedure.

The study by Kamuda, M. and Sullivan, C. J [12] demonstrates a neural network that uses all 1024 channels in the spectra. He also used simulations to create a large data set, although the number of instances was not reported. The performance of a single radionuclide is robust. However, when the spectra contain a mixture of radionuclides, the network predicts low probabilities for each radionuclide because the chosen architecture uses Softmax as the activation function. This activation function normalizes the output to sum up to one, but each neuron in the network output has independent probabilities of occurrence.

The method proposed in this study utilizes a vast data set for both training and testing. Using Sigmoid as the activation function enables the model to correctly predict different mixtures, from one radionuclide to up to four radionuclides.

The vast data set prepared for this study, using slightly different geometries and simulation parameters, generated a diverse data set that helped the model generalize in the test set, as shown in Figure 4.

ROC analysis shows robust performance; the model achieves near-zero false-positive rates using higher thresholds. The Ba-133 with Eu-152 test instance was correctly classified, corroborating the ROC analysis.

The model performance remains consistent across spectra with different start energies, which is crucial in our context, as the current tool (Genie 2000) requires calibration curve information. This model could allow IPEN's Radioactive Waste Management Department to characterize radioactive waste with fewer detector calibration cycles while maintaining the same accuracy.

Further tests are required using an experimental setup with a real source, drum, geometry, and equipment to validate the model's generalization. In addition, the ANSI standard [25] should be used for real experimental data.

4. CONCLUSIONS

A deep neural network model called VGG-19-γ was developed to identify several radionuclides in gamma spectra with robust performance. The model used simulated spectra from slightly different geometries and simulation parameters for training and testing. Data argumentation during the generation of new spectra with up to four different radionuclides drove the model to achieve robust performance.

Transfer learning helped to speed up this study, as the architecture was not built from scratch. Using Sigmoid as the activation function was crucial in creating a model with robust performance. Correct results are achieved on test data, whether in a single-radionuclide or a multiple-radionuclide spectrum. In the best scenario, further analysis of experimental data will confirm the method's robustness; in the worst scenario, it will highlight the weakness that needs to be addressed.

Finally, the architecture can be modified to output the activity per radionuclide, creating a model that performs classification and regression simultaneously.

ACKNOWLEDGMENT

We thank our colleagues from IPEN's Radioactive Waste Management Department, who provided insight and expertise that greatly assisted the research, although they may not agree with all the interpretations/conclusions of this paper. We thank Dr. José M. Fernández-Varea for the assistance with PENELOPE/penEasy code and customizations.

FUNDING

This study was financed in part by the Coordenação de Aperfeiçoamento de Pessoal de Nível Superior – Brasil (CAPES) – Finance Code 001".

CONFLICT OF INTEREST

All authors declare that they have no conflicts of interest.

REFERENCES

[1] LECUN, Y.; BENGIO, Y.; HINTON, G. Deep learning. **Nature**, Nature Publishing Group, v. 521, n. 7553, p. 436, 2015.

[2] SIMONYAN, K.; ZISSERMAN, **A. Very deep convolutional networks for large-scale image recognition**. arXiv preprint arXiv:1409.1556, 2014.

[3] HE, K. et al. **Mask r-cnn**. In: Proceedings of the IEEE international conference on computer vision. [S.l.: s.n.], 2017. p. 2961–2969.

[4] KALCHBRENNER, N. et al. **Neural machine translation in linear time**. arXiv preprint arXiv:1610.10099, 2016.

[5] GRAVES, A.; JAITLY, N. **Towards end-to-end speech recognition with recurrent neural networks.** In: International conference on machine learning. [S.l.: s.n.], 2014. p. 1764–1772.

[6] CHIU, C. et al. **State-of-the-art speech recognition with sequence-to-sequence models**. CoRR, abs/1712.01769, 2017. Disponível em: <http://arxiv.org/abs/1712.01769>.

[7] SUN, C. et al. **Revisiting unreasonable effectiveness of data in deep learning era**. In: The IEEE International Conference on Computer Vision (ICCV). [S.l.: s.n.], 2017.

[8] PAN, S. J.; YANG, Q. **A survey on transfer learning. IEEE Transactions on knowledge and data engineering**, IEEE, v. 22, n. 10, p. 1345–1359, 2009.

[9] KELLER, P. E. et al. **Nuclear spectral analysis via artificial neural networks for waste handling. IEEE transactions on nuclear science**, IEEE, v. 42, n. 4, p. 709–715, 1995.

[10] YOSHIDA, E. et al. Application of neural networks for the analysis of gamma-ray spectra measured with a Ge spectrometer. **Nuclear Instruments and Methods in Physics Research Section A: Accelerators, Spectrometers, Detectors and Associated Equipment**, 2002. ISSN 01689002.

[11] CHEN, L.; WEI, Y.-X. Nuclide identification algorithm based on k–l transform and neural networks. **Nuclear Instruments and Methods in Physics Research Section A: Accelerators, Spectrometers, Detectors and Associated Equipment**, v. 598, n. 2, p. 450 – 453, 2009. ISSN 0168-9002.

[12] KAMUDA, M.; SULLIVAN, C. J. An automated isotope identification and quantification algorithm for isotope mixtures in low-resolution gamma-ray spectra. **Radiation Physics and Chemistry**, Elsevier, v. 155, p. 281–286, 2019.

[13] Metropolis, N., & Ulam, S. (1949). The Monte Carlo method. **Journal of the American Statistical Association**, 44(247), 335-341.

[14] SEMPAU, J. **Peneasy, a structured main program from penelope**. Freely available from http://www. upc. es/inte/downloads/penEasy. htm, v. 2006, p. 06–01, 2006.

[15] Householder, Alston S. (June 1941). "A theory of steady-state activity in nerve-fiber networks: I. Definitions and preliminary lemmas". **The Bulletin of Mathematical Biophysics**. 3 (2): 63–69. doi:10.1007/BF02478220. ISSN 0007-4985.

[16] Bridle, John S. (1990a). Soulié F.F.; Hérault J. (eds.). Probabilistic Interpretation of Feedforward Classification Network Outputs, with Relationships to Statistical Pattern

Recognition. Neurocomputing: Algorithms, Architectures and Applications (1989). **NATO ASI Series** (Series F: Computer and Systems Sciences). 68. Berlin, Heidelberg: Springer. pp. 227–236. doi:10.1007/978-3-642-76153-9_28.

[17] Soti, Z., Magill, J., & Dreher, R. (2019). **Karlsruhe Nuclide Chart – New 10th edition 2018**. EPJ Nuclear Sciences & Technologies, 10(1), doi:10.1051/epjn/2024009.

[18] CHOLLET, F. et al. **Keras**. 2015. <https://keras.io>.

[19] ABADI, M. et al. **TensorFlow: Large-Scale Machine Learning on Heterogeneous Systems.** 2015. Software available from tensorflow.org. Disponível em: <https://www.tensorflow.org/>.

[20] NICKOLLS, J. et al. Scalable parallel programming with cuda. **Queue**, ACM, New York, NY, USA, v. 6, n. 2, p. 40–53, mar. 2008. ISSN 1542-7730.

[21] CHETLUR, S. et al. **cudnn: Efficient primitives for deep learning**. arXiv preprint arXiv:1410.0759, 2014.

[22] GARCÍA-TORAÑO, E.; PEYRES, V.; SALVAT, F. Pennuc: Monte carlo simulation of the decay of radionuclides. **Computer Physics Communications**, Elsevier, v. 245, p.106849, 2019.

[23] KINGMA, D. P.; BA, J. **Adam: A method for stochastic optimization**. In: BENGIO, Y.; LECUN, Y. (Ed.). 3rd International Conference on Learning Representations, ICLR 2015, San Diego, CA, USA, May 7-9, 2015, Conference Track Proceedings. [s.n.], 2015. Disponível em: <http://arxiv.org/abs/1412.6980>.

[24] FAWCETT, T. An introduction to ROC analysis. **Pattern Recognition Letters**, North-Holland, v. 27, n. 8, p. 861–874, jun 2006. ISSN 01678655.

[25] ANSI. **American National Standard Performance Criteria for Hand-Held Instruments for the Detection and Identification of Radionuclides**. [S.l.], 2007.

LICENSE